Peer-Reviewed Technical Communication

Performance of a MEMS IMU for Localizing a Seaglider AUV on an Acoustic Tracking Range

Wendy E. Snyder, Martin C. Renken, and Lora J. Van Uffelen

***Abstract*—A Seaglider instrumented with an inertial attitude and heading reference system was tracked for three days on an acoustic tracking range in Dabob Bay, Washington, operated by the Naval Undersea Warfare Center, Keyport, WA, USA. Inertial measurements were integrated to yield estimates of position and compared with tracked positions. Within 3 min, the integrated positioning results deviated from tracked positions by more than a kilometer. The addition of a depth constraint from pressure sensor measurements slowed the error growth over time, but even with this constraint, measurements were too noisy to accurately determine position without aid from additional sensors. Inertial data did contribute to accurate localization when used to estimate vehicle attitude and incorporated into an existing flight model; however, results did not demonstrate marked improvement over existing flight models. Although not a decisive demonstration of vehicle positioning with a standalone low-cost, low-power sensor, the results presented here provide a benchmark for comparison as MEMS inertial sensors continue to evolve using a valuable ground-truth of subsea Seaglider position not previously available.**

***Index Terms*—Attitude heading reference system (AHRS), autonomous underwater vehicle (AUV), Seaglider.**

I. Introduction

Surface vehicles and unmanned aerial vehicles can rely on positioning information from a global navigation satellite system (GNSS); however, since electromagnetic GNSS signals do not propagate far underwater, underwater vehicles rely on a combination of surface GNSS fixes, dead-reckoning, acoustic tracking, hydrodynamic models, and inertial navigation to find a position solution. Many types of autonomous underwater vehicles (AUVs) rely on inertial navigation systems (INSs) for localization and navigation when underwater for extended periods of time. INSs have not previously been used on glider-type AUVs due to the relatively high power requirements and large size of such systems compared to the low power and small payload capacity of glider platforms.

The Seaglider is a glider-type AUV commercially available from Huntington Ingalls Industries and is primarily used for profiling oceanographic quantities, such as temperature, salinity, and oxygen. It is capable of diving to 1000-m depth and can be underwater for several hours at a time. Ground truth positioning information is rarely available until the vehicle surfaces and obtains access to a GNSS, but subsea positions are estimated throughout a Seaglider dive with vehicle hydrodynamic models [1], [2].

For many glider applications, precise vehicle localization is generally not a critical concern. As the glider platform matures, there has been a growing interest in expanding its application and measurement capabilities. One such application is the use of gliders as mobile receivers for active acoustic signals including ocean acoustic tomography transmissions. The measurement of acoustic arrivals from an active acoustic source on a mobile receiver requires precise positioning information to resolve the fundamental ambiguity between position and sound speed. Position can be estimated from receptions of active acoustic source transmissions. In the Philippine Sea Tomography Experiment, glider position was estimated using acoustic sources at long ranges (hundreds of kilometers) with resulting root-mean-squared (rms) uncertainties on the order of 80 m [3], [4]; however, these position estimates require acoustic sources to be deployed, and the sources themselves typically only transmit every few hours.

Positioning solutions for the Seaglider vehicle have not made use of inertial measurements to the knowledge of the authors. Glider speeds are on the order of 20–25 cm/s, so typical low-magnitude sensors capable of measuring two g's of acceleration and 50–60 deg/s angular rates are capable of measuring the forces and rates expected in normal glider operation. The entire Seaglider vehicle can operate on 0.5 W (the Seaglider motto is "half a knot at half a Watt" [5]) and has limited sensor payload space. This limits the ability to integrate higher accuracy AUV INS systems onto the Seaglider; such as the iXblue Phins Compact Series, which require about 12–20 W and 0.5–6 L of volume [6].

Inertial measurement technologies have been available on the market since the 1970 s and 1980 s. With the small and inexpensive MEMS options developed since the mid-1990s, it is now becoming more feasible to integrate inertial measurement units (IMUs) on glider platforms. In the last 20–30 years, bias stability for microelectromechanical system (MEMS) units has improved from 18–300 deg/h to a range of 5–30 deg/h for low-end tactical applications. The number of parts required for such devices has also been reduced from over 100 in early gyroscope devices to just 1–3 components for more modern MEMS units [7], [8].

When aided by a Doppler velocity log (DVL), INSs are capable of achieving position error growth of $\sim$0.2% distance traveled (2σ) [9]. However, DVLs typically only operate within a few hundred meters of the seafloor and thus could not be used on a vehicle such as a Seaglider,

Manuscript received 12 November 2021; revised 20 April 2022; accepted 5 August 2022. The Seaglider deployment on the Dabob Bay Acoustic Tracking Range was made possible with support from the Naval Undersea Warfare Center Division Keyport, with additional project support provided by the Office of Naval Research under Grant N00014-17-1-2228: PI Lora Van Uffelen and Grant N00014-20-1-2040 and Grant N00014-22-1-2295: National Institute for Undersea Vehicle Technology (NIUVT). The work of W. E. Snyder was supported by the Science, Mathematics, and Research for Transformation scholarship program. This project was performed as part of W. E. Snyder's master's thesis. An earlier version of this paper was presented in part at the MTS/IEEE OCEANS Conference, 2019, Marseille, June 17–20, 2019 [DOI: 10.1109/OCEANSE.2019.8867252]. *(Corresponding author: Lora J. Van Uffelen.)*

Associate Editor: R. Bachmayer.

Wendy E. Snyder and Lora J. Van Uffelen are with the Department of Ocean Engineering, University of Rhode Island, Narragansett, RI 02882 USA (e-mail: wendy_snyder@my.uri.edu; loravu@uri.edu).

Martin C. Renken is with the Naval Undersea Warfare Center Division Keyport, Keyport, WA 98345 USA (e-mail: martin.renken@navy.mil).

Digital Object Identifier 10.1109/JOE.2022.3198474

Distribution A: Cleared for public release by NUWC Division Keyport

which operates in the mid-water column. Recent work has been done using the *Sirius*, *Sentry*, and *HUGIN* AUVs to improve mid-water localization using velocity estimates of ocean currents from acoustic Doppler current profilers (ADCPs) to aid IMUs [9], [10], [11]. While this concept is still under development, it has potential for the Seaglider platform, as ADCPs have been implemented the Seaglider platform to aid in navigation as well as to provide an estimate of ocean currents [12].

Recent field experiments have demonstrated an accurate navigation solution that utilizes MEMS IMU data coupled with vehicle dynamic model velocity and acoustic time-of-flight ranging measurements for two different AUVs: 1) the Iver2 and 2) the Bluefin Robotics SandShark [13].

As inertial measurement technology continues to improve with reductions in size and power requirements, understanding the potential for improvements to localization using inertial systems may be an important step toward improving localization accuracy for glider platforms.

A field experiment was performed on the Dabob Bay acoustic tracking range operated by the Naval Undersea Warfare Center (NUWC) Division Keyport, Keyport, WA, USA. The acoustically-tracked positions constitute an important data set, as it is difficult to obtain ground truth positioning data, and to our knowledge, no other such tracked data sets for Seaglider have been published. These data are used to investigate the viability of a low-cost, off-the-shelf, MEMS-based IMU for subsea glider positioning. Localization solutions resulting from direct integration of the IMU measurements are presented as well as positions that were integrated with the constraint of measured vehicle depth. Additionally, we investigate whether IMU measurements can be used to augment existing flight models. Seaglider pilots have access to two models to estimate Seaglider position between GPS fixes at the surface: the hydrodynamic model (HDM) and the glide-slope model (GSM). Advanced Seaglider pilots will tune coefficients used in the HDM during a mission, updating them as vehicle data are reported at each glider surfacing. A related paper addresses the evaluation of this hydrodynamic flight model for the Seaglider AUV using this data set [2]. Here, we use inertial measurements to estimate vehicle attitude for use as an input to the GSM, a simple and robust model that provides reasonable solutions even without fine tuning of hydrodynamic parameters.

The rest of this article is organized as follows. A description of the acoustic tracking experiment and collected data set are in Section II. Localization results derived from IMU data, including direct integration, integration constrained by vehicle depth, and IMU data used to augment the existing GSM flight model are in Section III. Discussion is given in Section IV. Finally, Section V concludes this article.

II. Data Collection

A Seaglider was deployed on the Dabob Bay acoustic tracking range from 24 to 27 September 2018. The Seaglider was deployed for a total of 68 h during which time it completed 86 dives. Of these dives, acoustic tracking data were available for 19 full dives, 3 of which were removed from analysis due to an atypical dive profile in which the glider hovered near the surface for a prolonged period of time before descending. Dive depths varied between 45 m and 126 m, limited by the depth of the acoustic tracking range.

In addition to the standard sensor package, a Lord 3DM-GX5-25 attitude and heading reference system (AHRS) was mounted inside the Seaglider pressure hull along with a Beaglebone Black datalogger used to log the inertial data during testing (see Fig. 1). The AHRS and datalogger were installed where the Seaglider ancillary battery is typically mounted. The ancillary battery was removed for this deployment.

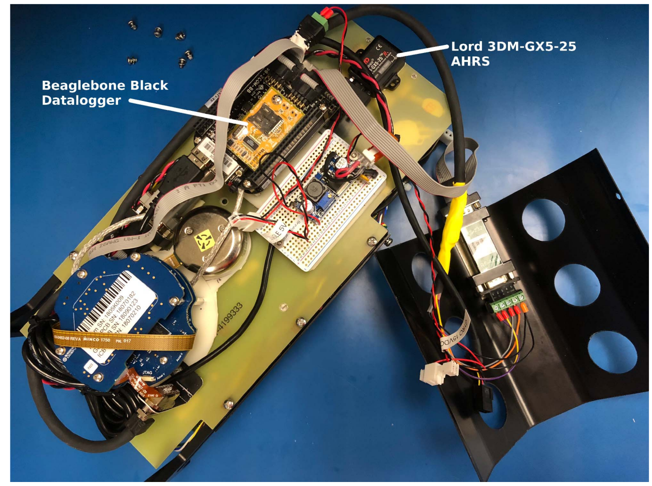

Fig. 1. Layout of the AHRS and datalogger on the Seaglider during the acoustic tracking experiment on Dabob Bay.

A. Seaglider Data

The Seaglider sensor package includes the Sparton SP3004D compass, Seabird conductivity and temperature (CT) sail, Kistler model 4260M060 pressure sensor, and Garmin 15H-W GPS receiver. The Seabird CT and pressure sensors were programmed to sample every 5 s throughout the deployment. The sampling rate of the Seaglider compass varied throughout each dive depending on processor availability but did not exceed 0.33 Hz.

At each surfacing, the Seaglider transmits dive data to a basestation computer via Iridium satellite connection. Data are compiled into a netcdf file for each dive and include measurements from the conductivity, temperature, and depth (CTD) and pressure sensors as well as surface GPS positions and position estimates from vehicle flight models. Additional information on the Seaglider flight model estimates is provided in [2].

B. Inertial Measurements

The Lord AHRS is a MEMS sensor comprised of magnetometers, accelerometers, and gyroscopes in all three axes, and was selected for its low-cost, low-power, and low-noise characteristics. The IMU was powered via the 15-V power supply on the Seaglider and was estimated to draw 0.5 W. Data were provided via a serial interface connected to an independent datalogger. Further details of the sensor selection and integration are outlined in [14]. The IMU data logging rate was 10 Hz.

Before deployment, the IMU was calibrated according to manufacturer recommended procedures. The Seaglider was leveled with the IMU installed and pitch and roll biases were zeroed. A magnetic compass calibration was performed using software provided by the manufacturer after installation on the vehicle. In-water compass calibration dives for the stock Seaglider compass were completed during the deployment.

During the experiment, raw magnetometer, accelerometer, and gyroscope measurements were collected. Additional data fields measuring the change in velocity and change in attitude angle, ΔV and $\Delta\Theta$, were recorded. These data fields calculate the change in velocity and the change in attitude from 100 accelerometer and gyroscope measurements (sampled at 1000 Hz), respectively, over a 0.1-s sample interval.

C. Ground Truth Positions From Acoustic Tracking Range

The Dabob Bay range is instrumented with short-baseline acoustic arrays, which were used to actively track the Seaglider during daytime operations. In this work, the acoustic track from the range, after applying the drift correction described below was assumed to be a ground-truth track from which the accuracy of different localization solutions was evaluated.

A self-powered acoustic pinger specific to the Dabob Bay acoustic tracking range was positioned in the aft payload bay of the Seaglider. At the outset of the Seaglider deployment, the acoustic pinger was synchronized with the range tracking system. The pinger was then resynchronized ~45.5 h into the 68-h deployment. The nominal ping interval was 4 s and the offset at resynchronization was measured to be 0.1 s. The average ping interval error (dt_p) was estimated to be 2.44 ms assuming a constant ping interval, resulting in the following localization error dr:

$$dr = N_p dt_p c_{\text{avg}} \tag{1}$$

where N_p is the ping number counted from the most recent synchronization, dt_p is the ping interval error, and c_{avg} is a harmonic average sound speed computed from range CTD data between the glider depth and array depth for each reception. The estimate of dr was subtracted from the range (i.e., distance) measurement of the raw tracking fix and used with the raw bearing measurement to compute the drift-corrected acoustic tracking location.

The drift-corrected track estimates were compared to the surface GPS fixes for ping times that occurred within 10 s of the GPS fixes. The average difference between the Seaglider GPS and range track position was 6.5 m, which is consistent with the expected accuracy of the GPS receiver.

Acoustic ray bending effects were found to be negligible for drift corrections based on ray tracing simulations performed with a CTD cast measured at the outset of the experiment. Horizontal position errors due to neglecting ray bending effects were estimated to be 0.1 m for steep launch angles (i.e., when the glider is shallow) with respect to the horizontal and 0.25 m for shallow ray launch angles (i.e., when the glider is deep).

The tracked positions in depth were corrected using measurements from the Seaglider's onboard pressure sensor, which provides more reliable and accurate depth measurements than the acoustic range track. Typical depth errors were 3.5–5 m. These errors could result from tidal variations (2–3 m during the deployment), the depth difference between the pressure sensor on the Seaglider and the pinger location, which varies as a function of vehicle orientation, and the straight ray assumption. Combined with the results of the comparison of surface track fixes to GPS, these results validate the accuracy of the corrected ground truth track.

III. Localization Solutions From IMU Data

Inertial measurements from the IMU were integrated to generate a localization solution for the Seaglider during each tracked dive. For the purposes of this article, we define a body frame b in which the x-axis points forward along the central (roll) axis of the vehicle, the y-axis points to the right of the central axis and aligns with the pitch axis of the vehicle, and the z-axis completes the orthogonal set pointing down (see Fig. 2). The local navigation frame n is defined such that the origin is located at the body frame origin, the x-axis points toward true north, the y-axis points toward true east and the z-axis aligns with the gravity vector pointing down. This local navigation frame is also commonly known as the North, East, Down (NED) frame.

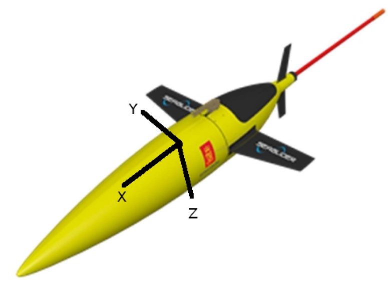

Fig. 2. Body coordinate frame defined for the Seaglider vehicle

A. Unconstrained Integration

Initial velocity was assumed to be zero at the start of the dive and initial position was determined from the GPS fix just before descent. The vehicle pitch and roll were initialized using accelerometer measurements in leveling equations. The leveling equations assume there is no linear acceleration such that accelerometers measure only gravitational acceleration. The leveling equations are expressed as

$$\phi = \arctan 2\left(-f_y^b, -f_z^b\right) \tag{2}$$

$$\theta = \arctan\left(\frac{-f_x^b}{\sqrt{(f_y^b)^2 + (f_z^b)^2}}\right) \tag{3}$$

where ϕ is the roll angle, θ is the pitch angle, $\arctan 2$ is the four-quadrant inverse tangent function, and $\mathbf{f}^b$ (sometimes expressed $\mathbf{f}_{ib}^b$) is the vector of specific force measured by the accelerometers expressed in the body frame where subscripts indicate the x, y, and z directional components [15].

The heading was initialized from the magnetometer measurements by fitting the magnetic vector to the earth's magnetic field vector at the location of operation. This estimation uses the pitch and roll estimates and is performed in two steps. First, the magnetic field vector as measured by the magnetometer in the body frame ($\mathbf{h}^b$) is rotated into the local navigation frame ($\mathbf{h}^n$) using

$$\mathbf{h}^n = \mathbf{C}_b^n(\phi, \theta, \psi = 0)\mathbf{h}^b \tag{4}$$

where $\mathbf{C}_b^n(\phi, \theta, \psi = 0)$ represents a direction cosine matrix (DCM, also called a rotation matrix) from the body frame to the local navigation frame with inputs for roll and pitch only (i.e., assuming a heading of zero) [16]. Then, the magnetic heading (ψ_m^b) is computed as

$$\psi_m^b = -\arctan 2\left(h_y^n, h_x^n\right) \tag{5}$$

where h_x^n and h_y^n are the x and y components of the measured magnetic field vector in the local navigation frame. The magnetic heading angle is referenced to the direction of magnetic north at the location of the measurement rather than geographical (true) north. The magnetic variation at the location of the measurement is added to the magnetic heading to reference to true north [15].

After initialization, attitude is updated by integrating the $\Delta\Theta$ measurements from the gyroscope at each time step. The new attitude is computed by updating the DCM according to the DCM update equation

$$\mathbf{C}_b^n(t+\tau) = \mathbf{C}_b^n(t)\left(\mathbf{I}_3 + \frac{\sin|\boldsymbol{\alpha}_{ib}^b|}{|\boldsymbol{\alpha}_{ib}^b|}[\boldsymbol{\alpha}_{ib}^b\wedge] + \frac{1-\cos|\boldsymbol{\alpha}_{ib}^b|}{|\boldsymbol{\alpha}_{ib}^b|^2}[\boldsymbol{\alpha}_{ib}^b\wedge]^2\right) \tag{6}$$

where $\mathbf{C}_b^n$ is shorthand for $\mathbf{C}_b^n(\phi, \theta, \psi)$, τ is the time step between gyroscope samples, $\boldsymbol{\alpha}_{ib}^b$ is the vector of attitude increments over the time

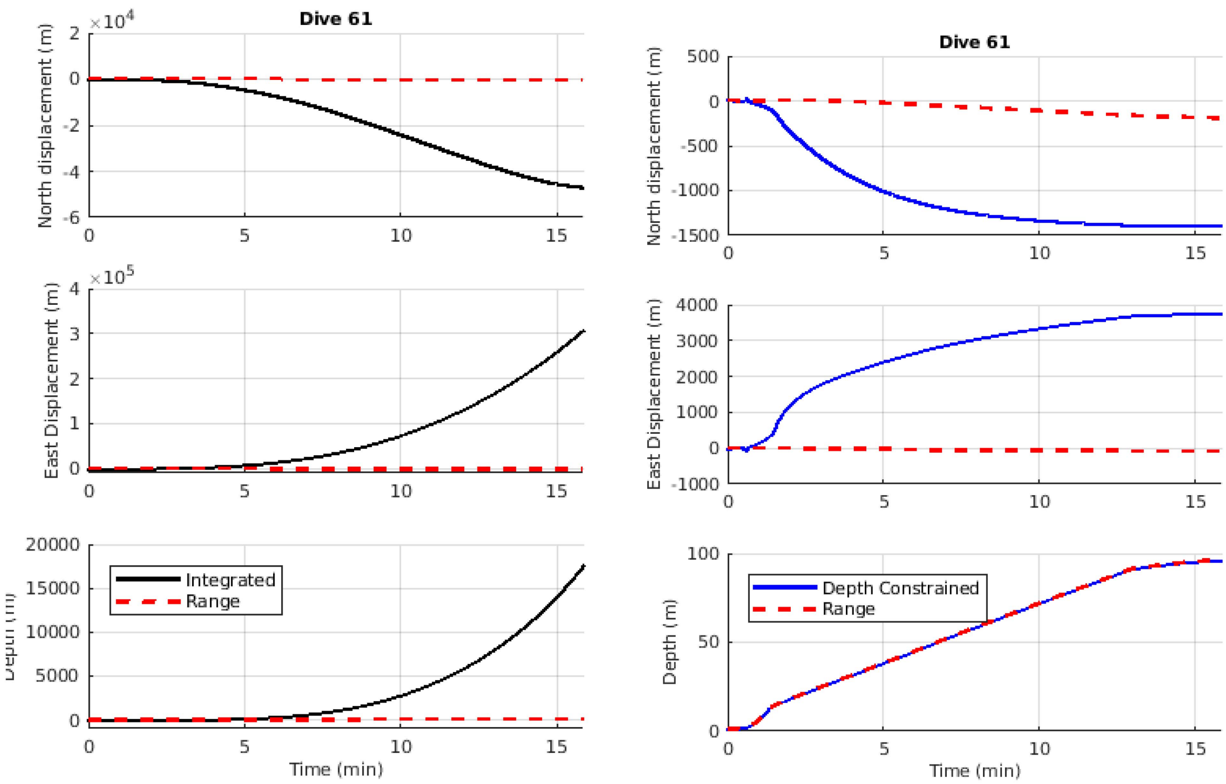

(a) (b)

Fig. 3. Vehicle track for the first half of Dive 61 computed from the range track and pressure sensor (dashed red). (a) Integration of the inertial data (solid black). (b) Depth-constrained integration of the inertial data (solid blue).

step ($\Delta\Theta$ measurements), and $[\boldsymbol{\alpha}_{ib}^{b}\wedge]$ represents a skew-symmetric matrix of attitude increments [15]. The DCM matrix can then be converted to a set of roll, pitch, and heading angles.

To get position estimates at each time step, the accelerometer measurements were rotated to the NED frame using the DCM and the gravitation acceleration was removed

$$\mathbf{a}_n = \mathbf{C}_b^n \mathbf{a}_b \tag{7}$$

$$\mathbf{a}_{\text{ln}} = 9.8(\mathbf{a}_n + \mathbf{g}) \tag{8}$$

where $\mathbf{a}_b$ is the vector of accelerations in the body frame (in units of g), $\mathbf{a}_n$ is the vector of accelerations in the NED frame (in units of g), $\mathbf{g}$ is the gravitational acceleration vector (in units of g), and $\mathbf{a}_{\text{ln}}$ is the linear vehicle acceleration in the NED frame (in m/s^2). Velocity and position updates were calculated according to

$$\mathbf{v}_{k+1} = \mathbf{v}_k + \mathbf{a}_{\text{ln}_k} * dt \tag{9}$$

$$\mathbf{r}_{k+1} = \mathbf{r}_k + \mathbf{v}_k * dt + 0.5 * \mathbf{a}_{\text{ln}_k} * dt^2 \tag{10}$$

where $\mathbf{v}_k$ is the vector of velocities in the NED reference frame at the $\mathbf{k}$th time-step index, $\mathbf{r}$ is the vector of the position in the NED frame, and dt is the time step between samples.

Because there was a short gap in data collection at the apogee of the dive, position data were only integrated for the first half of each tracked dive. An example of the integrated solution compared to the range track for a representative dive is shown in Fig 3(a).

The directly-integrated solution from the IMU quickly diverged from the ground truth position. These large errors result from the compounding of noise and bias in the accelerometer and gyroscope measurements. The integration of noise and bias in the gyroscope measurements creates a drift in the attitude estimate for the vehicle. When an inaccurate attitude is used to rotate accelerometer vectors into the NED frame, the resulting acceleration vectors are improperly aligned, creating artificial accelerations when gravity is removed and thereby contributing to additional drift in the integrated positions.

TABLE I
AVERAGE ERROR METRICS (WITH 1σ STANDARD DEVIATION)

	Max Error (m)	RMS Error (m)	Norm. Max Error (%)
Integrated	304,829 (219,786)	122,535 (84,098)	116,473 (77,701)
Depth Constrained	8,805 (13,484)	7,379 (12,892)	9,919 (19,753)
Thresh	23.6 (5.8)	13.7 (3.1)	4.6 (1.8)
GSM	23.3 (6.2)	13.3 (4.0)	4.5 (1.7)
HDM	18.9 (6.3)	11.5 (4.6)	3.7 (1.5)

The error in the integrated solution, or distance from the range track, was calculated for all dives [see Fig. 4(a)]. While the rate of error growth varies some between dives, most dives exhibit an exponential growth rate of error over time with solutions becoming unrealistic after a few minutes, and, in an extreme case, diverging by 780 km after about 20 min.

To quantify and compare the error in the various solutions, a set of error metrics was defined: the maximum error, the rms error, and the normalized maximum error. The maximum error was normalized by the distance traveled throughout the dive, as computed from the range track (see Table I).

B. Depth-Constrained Integration

As the depth of the vehicle was measured throughout the deployment with the vehicle pressure sensor, these data were used to constrain

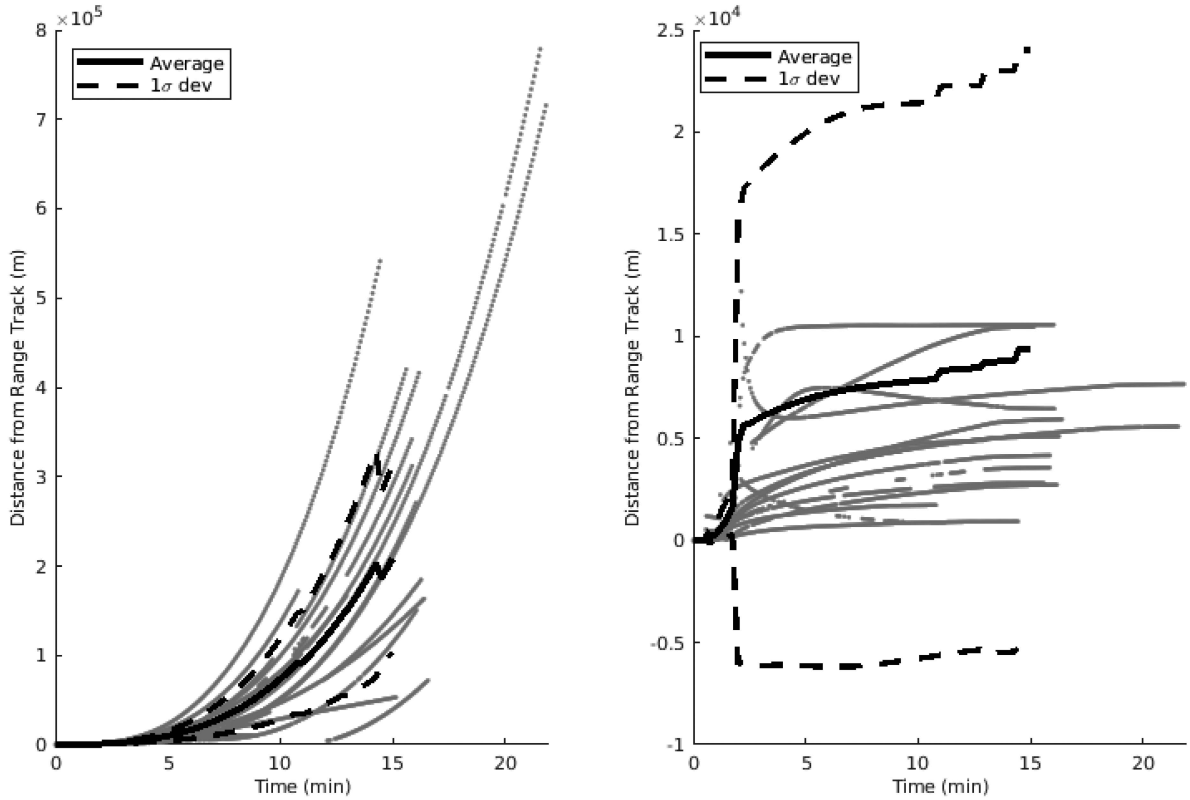

(a)

(b)

Fig. 4. Error in the integrated solutions as compared to the range track for the first half of all tracked dives as a function of time since the dive start (gray solid lines). Descent times for the 16 dives ranged from about 10 to 23 min. The average as a function of time (solid) and the 1σ deviation (dashed) are shown in black. (a) Integrated results. (b) Depth Constrained results. The scale of (b) does not capture the extent of the positioning error results from Dive 66, which differed from the range track by roughly 40–58 km between 2 and 16 min.

the velocities in the integration. The solution assumes drift in the accelerometers is the same in all three axes. The velocity vector computed using the integrated equations is converted into a magnitude and direction vector. Velocity magnitude was constrained when differences between integrated depths and depths derived from pressure exceeded a threshold value of 0.3 m, which is on the order of the uncertainty of the depth based on the measured pressure. The required velocity magnitude to achieve the pressure-based depth is

$$\mathrm{vmc} = \frac{1}{dt * v_{\mathrm{dir},z}} * (zp_{i+1} - pc_{z,i}) \tag{11}$$

where vmc is the constrained velocity magnitude, dt is the time step between samples, $v_{\mathrm{dir},z}$ is the z component of the velocity direction vector, zp_{i+1} is the pressure-based depth at the current time step, and $pc_{z,i}$ is the z component of the constrained position at the previous time step. The introduction of the threshold value provided a nonzero initialization of $v_{\mathrm{dir},z}$ in (11).

The constrained velocity vector vc is computed as

$$\mathrm{vc} = \mathrm{vmc} * v_{\mathrm{dir}} \tag{12}$$

where v_{dir} is the velocity direction vector. The constrained position is computed from (10) with the previous constrained position and the constrained velocity from (12) in place of integrated previous position and velocity.

Results of the depth-constrained integrated solution for a representative dive are shown in Fig. 3(b) for comparison with the unconstrained results for the same dive in Fig. 3(a). The vertical position is essentially identical to the pressure sensor depth, as dictated by the constraint.

The total distance from the range track (localization error) versus dive time was computed over the first 15 min of the dive for both the straight integration and the depth-constrained solution. These values were plotted over the data from all the dives. The average integrated error grows rapidly with increasing time for the unconstrained integrated solution while the error in the depth-constrained solution grows most rapidly in the first few minutes of the dive and then slows. While initial error growth is rapid, the depth constraint significantly reduces the magnitude of error overall [see Fig. 4(b), note the y-axis scale]. However, even with the depth constraint, the magnitude of the errors is not insignificant.

C. IMU Data Augmentation in Existing Flight Models

Low-cost IMUs, such as the one used for this experiment, are often used solely to estimate vehicle attitude and heading. Here, the attitude estimates derived from the IMU data were used as inputs to the Seaglider GSM solution to generate localization solutions for each tracked dive.

The Seaglider GSM uses attitude measurements and vertical velocity measurements from the pressure sensor to estimate the glide slope (pitch plus angle of attack) and horizontal speed of the Seaglider during a dive. Estimates of glide slope are determined using a model for the vehicle that incorporates hydrodynamic constants for lift and drag. In this experiment, hydrodynamic constants were based on estimates from the automated flight model system [2], [17]. The GSM model dead-reckons using the derived estimates of horizontal speed along with heading measurements and GPS fixes to obtain localization estimates [1], [14].

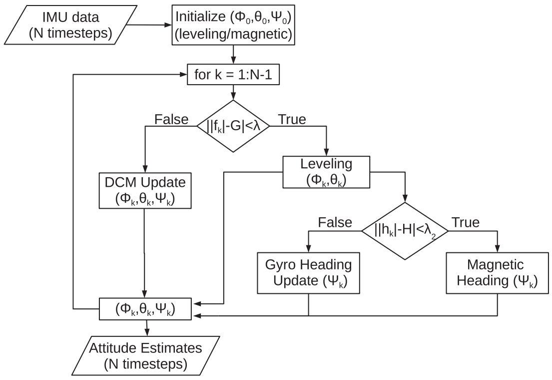

Fig. 5. Threshold algorithm flowchart.

In addition to the increased data sampling rate relative to the stock compass, the IMU has the advantage that it includes gyroscope measurements. However, calibrated magnetometer measurements from the Seaglider stock compass were used in place of magnetometer measurements from the IMU, as it was determined that the IMU magnetometer may have been influenced by the magnetic field of the battery that acts as a mass shifter in the Seaglider. At the battery's most forward point, it was about 36 cm from the IMU.

An attitude integration algorithm uses thresholds to determine whether to rely on accelerometer or gyroscope measurements for attitude at each data point (see Fig. 5). Inputs to the algorithm consist of the raw IMU data including accelerometer (ΔV), gyroscope ($\Delta\Theta$), and magnetometer measurements. Leveling and magnetic heading equations [(2), (3), (4), and (5)] were used on the first set of data points to provide an initial attitude estimate. The algorithm loops through each set of measurements and determines an attitude estimate for each time step. Since leveling is most reliable in the absence of linear acceleration, the algorithm first attempts to detect any linear acceleration present by comparing the magnitude of the measured acceleration vector ($|\mathbf{f}|$) to the known magnitude of gravitational acceleration (G = 1 g $\approx$ 9.81 m/s^2). If the difference between the measured magnitude and the expected magnitude is larger than a selected threshold ($\lambda = 0.01$ g), linear acceleration is present. The attitude expressed as Euler angles (roll, pitch, and yaw) is converted to a DCM, then updated from the measured $\Delta\Theta$ values using the DCM update equation (6). If the acceleration difference does not exceed the threshold (λ), leveling equations (2) and (3) determine the roll and pitch angles from accelerometer measurements. Note that a 1.6 deg offset was applied to measured pitch values to account for sensor alignment.

Magnetic headings are most reliable in the absence of both linear acceleration and magnetic disturbance [15]. In the case where linear accelerations are detected, the heading is also updated as part of the DCM update. However, if no linear acceleration is detected, the algorithm compares the magnitude of the measured magnetic field ($|\mathbf{h}|$) to the expected magnetic field magnitude ($H = 0.534$ G), based on the World Magnetic Model [15] for the Dabob Bay region. If the difference between the measured magnetic field strength exceeds a threshold ($\lambda_2 = 0.05$ G), a magnetic disturbance is considered present and $\Delta\Theta$ measurements are used to update the heading estimate according to

$$\psi(t+\tau) = \psi(t) + (\sin\phi\sec\theta)\alpha_y + (\cos\phi\sec\theta)\alpha_z \tag{13}$$

where $\psi(t)$ is the heading at the previous time step t [18]. If a magnetic disturbance is not detected, the heading is updated using the magnetometer data in (4) and (5). Each iteration of the loop outputs a set of attitude measurements based on raw IMU measurements during that time step. Since the stock compass had a slower time-varying sample rate, the gyroscope-based heading update was applied at time steps where magnetometer measurements were not available. A comparison of the attitude and heading components from the integrated method, threshold method, and stock compass is shown in Fig. 6. The threshold algorithm gives fairly identical results to the Seaglider stock compass while the integrated method has noticeable drift, particularly apparent in the second half of the dive.

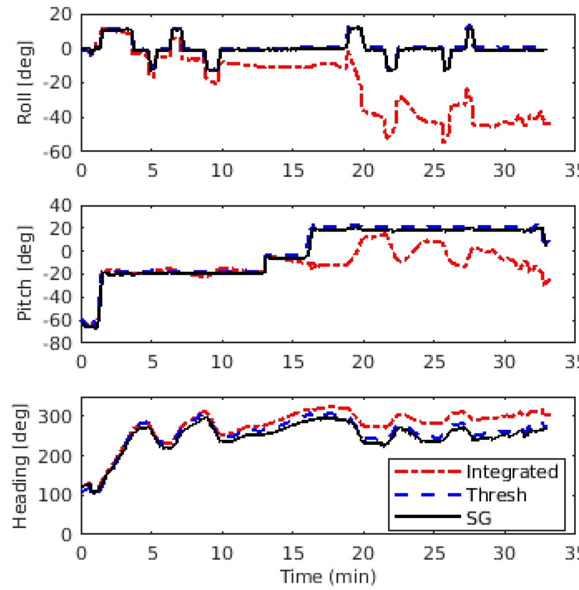

Fig. 6. Comparison of the attitude estimates for dive 61 from the Seaglider stock compass (black), integrated solution (red), and threshold attitude estimator (blue). Both the stock compass and threshold attitude estimators use calibrated magnetometer measurements from the stock compass.

While there is variability across different dives, Fig. 7 shows one example of the positioning solution using the Threshold algorithm attitude estimation from inertial measurements incorporated into the GSM flight model in comparison with the standard GSM and HDM flight model solutions based on the work in[2]. The error metric values for each of the individual tracked dives for these three solutions are shown in Fig. 8 and the averaged values of the metrics for all solutions are listed in Table I along with their 1σ standard deviations.

Note that two other attitude estimators were implemented as well, including a Kalman filtering algorithm and a tilt algorithm that utilized the same attitude estimation methods as the Seaglider currently uses for the stock compass data. The Kalman filtering solution was based on the method of Li and Wang [16], which was specifically developed considering low-cost/low-accuracy MEMS-type IMUs making it a good option for the Seaglider application. The results from these other two estimators were comparable to the threshold method described here and are, therefore, not presented.

The results presented in Table I show that the position estimates based on the attitude calculated using the threshold method were comparable to the existing GSM model results but did not improve upon them. Also, the HDM solution did average slightly lower error metrics than all other solutions, with similar or slightly higher standard deviations.

IV. Discussion

As evidenced by Fig. 4(a), the integrated solutions quickly drifted from the ground truth positions with errors growing exponentially for

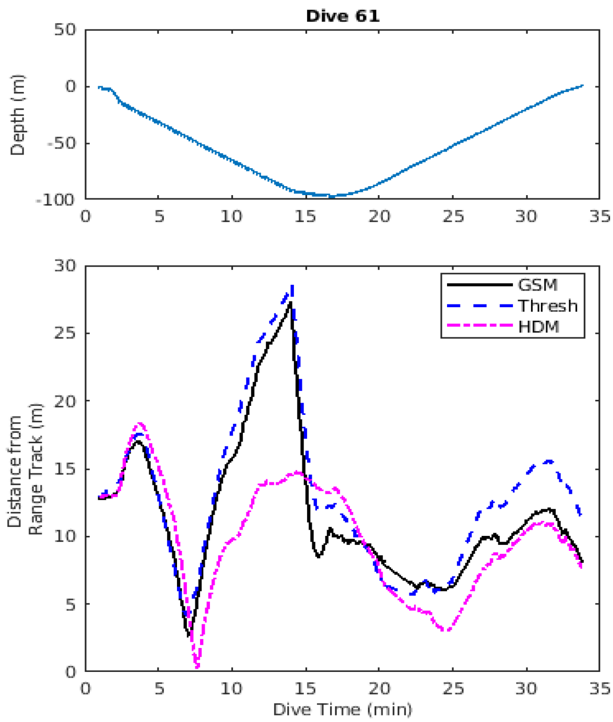

Fig. 7. Depth versus time (upper) and distance of all model-based solutions from the acoustic ground truth range track (lower) for Dive 61. Results are shown for the Seaglider GSM (black), the GSM using threshold attitude estimator (blue), and Seaglider HDM (magenta).

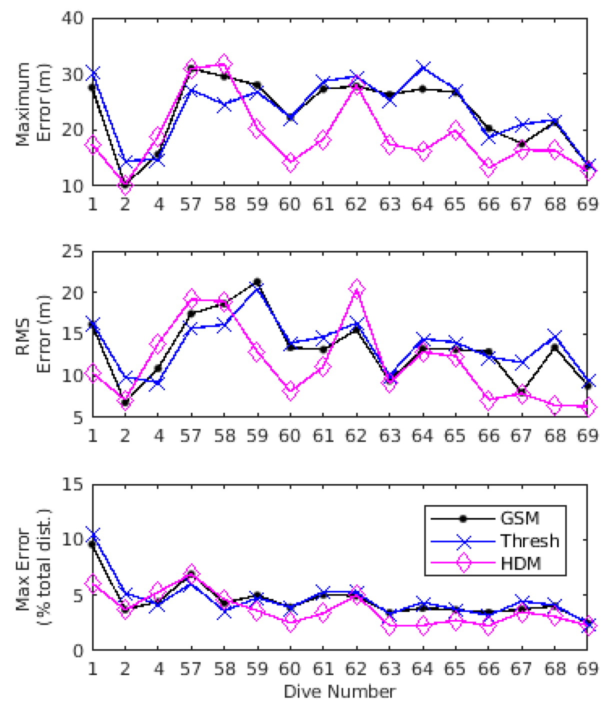

Fig. 8. Error metric values for each tracked dive using the model-based solutions. Results are shown for the Seaglider GSM (black), the GSM using threshold attitude estimator (blue), and Seaglider HDM (magenta).

most dives. Positioning results significantly improved with time when the position was constrained by pressure data collected by the vehicle. Fig. 4(b) showed that with the addition of a depth constraint errors still increased rather sharply during the first few minutes, for many dives around the 2-min mark, but error growth slowed as the dive continued.

It may be feasible to use models and/or other assumptions about the movement of the Seaglider to further constrain the inertial data. In both the depth-constrained and unconstrained positioning results, artificial accelerations result from the compounding effect of slight attitude errors with the removal of gravity. Artificial accelerations also create errors in the acceleration direction vector as artificial accelerations do not affect all directions equally. The depth constraint does not completely correct for these errors and effects, and additional measurements (or models) and constraints would be required to compensate for such errors. Magnetometer measurements could potentially be incorporated as an additional source of independent measurements. MEMS IMU magnetometers are notoriously susceptible to the surrounding magnetic environment; however, recent simulation work shows promise for providing effective calibration solutions [19]. Simulations using nonlinear mathematical models also show promise for estimating initial attitude and biases in MEMS inertial sensors for AUV applications [20]. To use magnetometers for heading, the pitch and roll angles must be known and the resulting heading would only constrain one set of rotations making such a constraint complex to formulate and apply.

Fiber optic gyroscopes (FOGs) have the potential to provide more stable gyroscope measurements, which would reduce the rate of drift in integrated attitude estimates. These improved attitude estimates would in turn improve velocity and position estimates as it enables gravitational acceleration to be properly removed from accelerometer data preventing artificial accelerations. In the last 10 years or so, bias stability in FOGs has been reduced from about 2 deg/h to 0.01 deg/h and coil size has been reduced to about a 2.5-cm diameter. FOGs are often used in larger and more power-hungry INS systems, which is a complicating factor for the low-power Seaglider platform. There are smaller 3-axis fiber optic gyros already available on the market such as the DSP-1760 Fiber Optic Gyro from KVH Technologies. While such sensors might be compact enough to fit into the Seaglider payload, they require upwards of 5W power, which is 10 times what a Seaglider would typically use. FOGs of this quality are also not sensitive enough to fully gyro-compass, i.e., to determine heading from measurements of Earth's rotation. Thus the accuracy of the attitude still relies upon accurate initialization from a magnetic compass and tilt sensor. Additionally, for longer term accurate inertial solution, typically a form of velocity or position update is required for fusion with inertial data through a Kalman filter or a related data fusion algorithm.

Much of this report focused on the accuracy of localization solutions using different types of inertial measurements, but there are a few other important factors that also affect localization accuracy for the Seaglider platform. While GPS is often heavily relied upon as a source of accurate positioning, there can still be a fair amount of uncertainty in the GPS fix, which can affect the overall accuracy of localization solutions. The average of the horizontal position error reported by the GPS across all 86 dives was 8.3 m with a standard deviation of 1.9 m. Compared to range data when the range fix was within 5 s of the GPS fix time, the average distance between the GPS fix and range fix was 7.3 m with a standard deviation of 3.5 m. These offsets affect the accuracy of the initialization and can create an initial bias in the localization solution.

In addition, the Seaglider processor takes about a minute from the time of the final GPS fix before a dive until it starts logging data for the current dive. During this time, the Seaglider sits at the surface and is subjected to movement by currents and wind. Thus, any bias offset introduced by the uncertainty of the initial GPS fix can be further increased during this period of unaccounted-for surface drift between the GPS fix and the initialization of other sensors. To fully take advantage of an inertial integrated solution, data would need to be collected continuously to avoid such gaps. In the case of the flight model-based solution, the period of surface drift could be modeled using the assumption that the rate of surface drift between subsequent surface GPS fixes is constant and extrapolating the starting dive location in time. Such consideration is not part of the standard GSM model but the correction is applied in [2].

Although vehicle flight models do not incorporate direct measurements of ocean currents, vehicle motion due to currents is accounted for as a single-depth-averaged current (DAC) calculated at the end of each dive, and vehicle positions estimated from the flight models are adjusted accordingly [1]. Unmeasured currents also contribute to uncertainty in vehicle position underwater. Recent work with the Petrel-L glider demonstrated improved localization performance when current estimates from an ocean model were incorporated with the DAC [21]. Dabob Bay experiences substantial tidal exchanges, and estimates of currents during this experiment based on a comparison of a hydrodynamic flight model and the acoustic range track are also presented in [2]. The reality of ocean navigation is that currents will be present everywhere in the ocean, and thus, ideal localization solutions would be robust to the presence of ocean currents.

V. Conclusion

The novel data set reported here is valuable to the community as ground-truth underwater positioning data are not readily available for the Seaglider platform, which typically operates over large spatial scales without access to GPS positioning except during surfacing events often separated by several hours. The inertial measurements described here were used in three different ways to estimate the position of the Seaglider: directly integrated, integrated with a depth constraint imposed by measurements from the vehicle pressure sensor, and used to estimate vehicle attitude, which was input into an existing flight model.

It is clear from the results presented here that the integration of MEMS-based inertial data cannot yet be relied upon for accurate localization in GPS-denied environments for any significant length of time. Constraining the measurements with pressure sensor data improved the results somewhat, but the positions typically deviated from the ground truth positions by a kilometer or more within the first 3 min of a dive.

MEMS-based inertial measurement systems were shown to be able to effectively provide attitude estimates, at least in this instance of low-acceleration Seaglider motion. Attitude estimates derived from the inertial data that were used with a simple flight models were able to produce reasonable position estimates; however, they did not outperform positioning estimates from existing flight models that incorporate measurements from a stock compass.

The Seaglider vehicle is unique as it has the limited payload and power available and also typically operates in mid-water where typical sensors that are used to aid inertial sensors, such as a DVL are not useful. As inertial technology continues to advance, lower power, lower noise, inertial measurement systems that can meet the space and power requirements of a Seaglider may be able to provide a reliable integrated navigation solution; however, an aided inertial system with some form of velocity or position updates incorporated from measurements or flight models would likely be more realistic than a stand-alone inertial system in the foreseeable future.

The results presented indicate that currently the hydrodynamic flight models, when properly tuned, still provide the best available estimate of underwater Seaglider position in the absence of an acoustically tracked solution. Although ground-truth data are difficult to obtain, data collected at calibrated acoustic tracking facilities offer valuable insight into vehicle position and dynamics underwater where GNSS localization is unavailable.

Acknowledgment

The authors would like to thank the Seaglider group at Huntington Ingalls Industries for their assistance with the integration of the sensor and datalogger on the Seaglider. Additional thanks to Jim Bennett, Charlie Eriksen, and Fritz Stahr in the Seaglider group at the University of Washington for their valuable insights and advice.

References

[1] C. C. Eriksen et al., “Seaglider: A long-range autonomous underwater vehicle for oceanographic research,” *IEEE J. Ocean. Eng.*, vol. 26, no. 4, pp. 424–436, Oct. 2001.

[2] J. Bennett, F. Stahr, C. C. Eriksen, M. C. Renken, W. E. Snyder, and L. J. Van Uffelen, “Assessing Seaglider model-based velocity and positioning accuracy on an acoustic tracking range,” *J. Atmosph. Ocean. Technol.*, vol. 38, pp. 1111–1123, 2020.

[3] L. J. Van Uffelen, B. M. Howe, E. M. Nosal, G. S. Carter, P. F. Worcester, and M. A. Dzieciuch, “Localization and subsurface position error estimation of gliders using broadband acoustic signals at long range,” *IEEE J. Ocean. Eng.*, vol. 41, no. 3, pp. 501–508, Jul. 2016.

[4] L. J. Van Uffelen et al., “Estimating uncertainty in subsurface glider position using transmissions from fixed acoustic tomography sources,” *J. Acoust. Soc. Amer.*, vol. 134, pp. 3260–3271, 2013.

[5] C. C. Eriksen and M. J. Perry, “The nurturing of Seagliders by the national oceanographic partnership program,” *Oceanography*, vol. 22, pp. 146–157, 2009.

[6] iXBlue, “Phins Compact Series Specifications,” 2019-05-DS-Phins CompactSeries datasheet, May 2019. [Online]. Available: https://www.ixblue.com/wp-content/uploads/2022/01/phins-compact-series-datasheet.pdf

[7] V. M. N. Passaro, A. Cuccovillo, L. Vaiani, M. De Carlo, and C. E. Campanella, “Gyroscope technology and applications: A review in the industrial perspective,” *Sensors*, vol. 17, pp. 2284–2305, 2017.

[8] R. L. Greenspan, “Inertial navigation technology from 1970-1995,” *J. Inst. Navigat.*, vol. 42, pp. 165–185, 1995.

[9] L. Medagoda, S. B. Williams, O. Pizarro, J. C. Kinsey, and M. V. Jakuba, “Mid-water current aided localization for autonomous underwater vehicles,” *Auton. Robots*, vol. 40, pp. 1207–1227, 2016.

[10] Hegrenæs and O. Hallingstad, “Model-aided INS with sea current estimation for robust underwater navigation,” *IEEE J. Ocean. Eng.*, vol. 41, no. 3, pp. 501–508, Jul. 2011.

[11] J. M. Stanway, “Dead reckoning through the water column with an acoustic Doppler current profiler: Field experiences,” in *Proc. IEEE OCEANS Conf.*, 2011, pp. 1–8.

[12] J. Jonker, A. Shcherbina, R. Krishfield, L. Van Uffelen, A. Aravkin, and S. E. Webster, “Preliminary results in current profile estimation and Doppler-aided navigation for autonomous underwater gliders,” in *Proc. IEEE OCEANS Conf.-Marseille*, 2019, pp. 1–8.

[13] J. H. Kepper, B. C. Claus, and J. C. Kinsey, “A navigation solution using a MEMS IMU, model-based dead-reckoning, and one-way-travel-time acoustic range measurements for autonomous underwater vehicles,” *IEEE J. Ocean. Eng.*, vol. 44, no. 3, pp. 664–682, Jul. 2019.

[14] W. Snyder, L. Van Uffelen, and M. Renken, “Effects of incorporating inertial measurements on the localization accuracy of the Seaglider AUV,” in *Proc. IEEE OCEANS Conf.*, 2019, pp. 1–6.

[15] P. D. Groves, *Principles of GNSS, Inertial, and Multisensor Intergrated Navigation Systems*. Norwood, MA, USA: Artech House, 2008.

[16] W. Li and J. Wang, “Effective adaptive Kalman filter for MEMS-IMU magnetometers integrated attitude and heading reference system,” *J. Navigat.*, vol. 66, pp. 99–113, 2013.

[17] J. Bennett, F. Stahr, and C. C. Eriksen, “Determining Seaglider velocities automatically,” Dept. Oceanogr., Univ. Washington, Tech. Rep., Aug. 2019, Art. no. 50. [Online]. Available: http://hdl.handle.net/1773/44948

[18] J. Diebel, “Representing attitude: Euler angles, unit quaternions, and rotation vectors,” Stanford Univ., Stanford, CA, USA, 2006.

[19] R. Yan, F. Zhang, and H. Chen, “A MEMS-based magnetometer calibration approach in AUV navigation system,” in *Proc. IEEE OCEANS Conf.*, 2019, pp. 1–6.

[20] D. Yuan, X. Ma, Y. Liu, and C. Zhang, “Dynamic initial alignment of the MEMS-based low-cost sins for AUV based on unscented Kalman filter,” in *Proc. IEEE OCEANS Conf.*, 2016, pp. 1–6.

[21] R. Zhang, W. Gao, S. Yang, Y. Wang, S. Lan, and X. Yang, “Ocean current-aided localization and navigation for underwater gliders with information matching algorithm,” *IEEE Sensors J.*, vol. 21, no. 22, pp. 26104–26114, Nov. 2021.

Wendy E. Snyder received the B.S. degree in mechanical engineering from the University of Rochester, Rochester, NY, USA, in 2017, and the M.S. degree in ocean engineering from the University of Rhode Island, Kingston, RI, USA, in 2019.

During the summers, she was a Remotely Operated Vehicle Pilot on the Exploration Vessel Nautilus.

Martin C. Renken received the B.S. degree in electrical engineering from Valparaiso University, Valparaiso, IN, USA, in 1991, and the Ph.D. degree in electrical engineering from the University of Colorado, Boulder, CO, USA, in 2001.

He is currently an Engineer and a Scientist with Naval Undersea Warfare Center Division Keyport Washington, Keyport, WA, USA. He has been a long-time civilian employee of the US Navy, applying signal-processing-based analysis to underwater problems. His research interests include underwater acoustics, underwater communications, test and evaluation of underwater systems and vehicles, and lately test and evaluation of autonomous underwater vehicles.

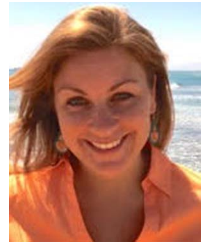

Lora J. Van Uffelen received the B.S. degree in engineering from Hope College, Holland, Michigan, in 2002 and the Ph.D. degree in oceanography from the Scripps Institution of Oceanography, University of California San Diego, San Diego, CA, USA, in 2009.

She is currently an Assistant Professor with the Department of Ocean Engineering, University of Rhode Island, Narragansett, RI, USA. She has participated in more than 20 research cruises with more than 400 days at sea. Her primary research interests include underwater acoustic propagation, acoustic positioning and navigation, and oceanographic instrumentation and technology.

Dr. Van Uffelen is a member of the Acoustical Society of America and the IEEE Oceanic Engineering Society.